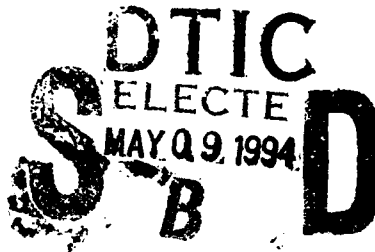# AD-A279 413

April 8, 1994   Reprint

Evaluation of a Hadamard-Coded Photodiode-Array
Spectrometer Under Low Illumination

PE 62101F
PR 3054
TA 01
WU 09

Joseph L. Robichaud*, Wallace K. Wong**,
Roger A. Van Tassel

Phillips Lab/GPO
29 Randolph Road
Hanscom AFB, MA 01731-3010

DTIC
ELECTE
MAY 0 9 1994
B
S D

PL-TR-94-2118

*Optical Systems Solutions, Inc., 50 Dalton Street, Tewksbury,
MA 01876 **SSG, Inc., 150 Bear Hill Road, Waltham MA 02154

Approved for public release; Distribution unlimited

Hadamard spectrometers are well known for their multiplexing and or throughput advantages. Traditionally these instruments require moving entrance and/or exit masks. The performance of a breadboard photodiode-array Hadamard transform spectrometer with a stationary entrance mask is evaluated against the same instrument configured with a single entrance slit. The higher throughput of the multislit, no-moving-parts instrument has provided a higher signal-to-noise ratio over the single-slit spectrometer in low-illumination conditions. Sources of noise are examined for the single-slit and multislit Hadamard instruments, and improvements for future designs are suggested.

94-13701

14. SUBJECT TERMS			15. NUMBER OF PAGES
Hadamard transform, Spectroscopy, High throughput			7
			16. PRICE CODE

17. SECURITY CLASSIFICATION OF REPORT	18. SECURITY CLASSIFICATION OF THIS PAGE	19. SECURITY CLASSIFICATION OF ABSTRACT	20. LIMITATION OF ABSTRACT
UNCLASSIFIED	UNCLASSIFIED	UNCLASSIFIED	SAR

94 05 05 156

Evaluation of a Hadamard-coded photodiode-array spectrometer under low illumination

Joseph L. Robichaud, Wallace K. Wong, and Roger A. Van Tassel

Hadamard spectrometers are well known for their multiplexing and or throughput advantages. Traditionally these instruments require moving entrance and/or exit masks. The performance of a breadboard photodiode-array Hadamard transform spectrometer with a stationary entrance mask is evaluated against the same instrument configured with a single entrance slit. The higher throughput of the multislit, no-moving-parts instrument has provided a higher signal-to-noise ratio over the single-slit spectrometer in low-illumination conditions. Sources of noise are examined for the single-slit and multislit Hadamard instruments, and improvements for future designs are suggested.

Key words: Hadamard transform, spectroscopy, high throughput.

Introduction

The application of Hadamard transform techniques in spectroscopy has provided throughput and/or multiplexing advantages compared with traditional single-slit spectrometers.[1,2] While a single-slit spectrometer can capture all the spectral components simultaneously by the use of a photodiode array in the exit plane, the throughput of the instrument is still severely limited by the small area of the entrance aperture.

Improved throughput has been obtained by application of large-area, spatially encoded masks at the entrance and/or exit planes. These multislit instruments use a single detector and moving entrance or exit masks. Doubly encoded designs with N entrance and N exit slits require $2N - 1$ measurements.[3] More recently a Hadamard-coded entrance mask, photodiode-array instrument has been proposed and demonstrated; it has the advantage of no moving parts.[4,5] The instrument has a theoretical throughput advantage over a traditional single-slit spectrometer since $\sim N/2$ open slits are used to image radiation onto the detector array. The design does not require interferometric tolerances, and, having no moving parts, it is inherently more rugged than a scanning system. Additionally, the spectrometer measures all the spectral elements simultaneously, providing the capability of measuring randomly occurring pulse sources.

Theoretical Comparison with a Single-Slit Spectrometer

Comparison of the Hadamard design with a conventional single-slit, photodiode-array spectrometer is illustrated in Fig. 1. We describe the single-slit spectrometer to introduce notation that is useful in describing the Hadamard design.

Single-Slit Photodiode-Array Spectrometer

In the single-entrance-slit instrument the optical separator disperses the incoming radiation and forms an image of the entrance slit at the focal plane. The location of this image is determined by the wavelength of the incoming radiation. Multiple images are formed by polychromatic radiation, and the spectrum is obtained directly from the output of the array. An estimate of the energy $E(n)$ is given directly by the signal on the corresponding detector $D(n)$ by

$$D(n) = E(n) + e(n), \qquad (1)$$

where n is an index over the number of spectral elements N and $e(n)$ is the detector noise associated with the nth detector. In this single-slit instrument the energy of the nth spectral element is estimated by

$$\langle E(n) \rangle = D(n), \qquad (2)$$

and the difference between the estimate and the

J. L. Robichaud is with Optical Systems Solutions, Inc., 50 Dalton Street, Tewksbury, Massachusetts 01876; W. K. Wong is with SSG, Inc., 150 Bear Hill Road, Waltham, Massachusetts 02154; R. A. Van Tassel is with the Geophysics Directorate, Phillips Laboratory Geophysics Directorate, Optical Environmental Division, Hanscom Air Force Base, Massachusetts 01731.
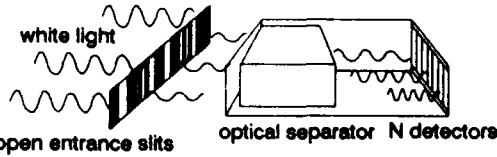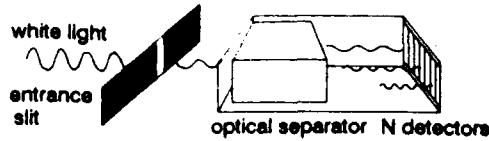
94 5 05 156

Fig. 1. Comparison of a conventional single-slit, photodiode-array spectrometer and a Hadamard transform spectrometer (HTS).

energy is

$$\langle E(n) \rangle - E(n) = e(n). \tag{3}$$

We can use Eq. (3) to form an expression for the theoretical signal-to-noise ratio (S/N) expected from the single-slit spectrometer as

$$S/N_{single\ slit} = E(n)/e(n). \tag{4}$$

Hadamard Transform Photodiode-Array Spectrometer

In the Hadamard design presented here, a Hadamard mask with $2N - 1$ slits is placed at the front focal plane of a spectrometer and is used as the entrance aperture for the system. The pattern, or coding, of the Hadamard mask is based on repeating the first row of a circulant S matrix as described by Harwit and Sloane.[6] For monochromatic radiation a mirror image of the mask is produced at the back focal plane. The position of this image is determined by the wavelength of the incoming beam. For polychromatic radiation, multiple images are superimposed on the detector array. A general expression for the detector output is given by

$$D(n) = e(n) + \sum_{j=0}^{N-1} E(j + 1)S[j + N - (n - 1)], \tag{5}$$

where j is an index over the N spectral elements and $S(j)$ represents the encodement of the $2N - 1$ slit positions.

For illustration we consider the case of $N = 7$. For $N = 7$ there are 13 individual slits. We model an idealized optical system where a mirror image of the entrance mask is perfectly reproduced at the exit plane. In addition, we assume that the instrument is linearly shift invariant so that a change in wavelength of the incoming radiation by $m\delta\lambda$ will shift the image of the mask by exactly m pixels, where m is an integer from 1 to N. We can apply Eq. (5) to this idealized instrument along with the Hadamard encodement,[6]

$$1\ 1\ 1\ 0\ 1\ 0\ 0\ 1\ 1\ 1\ 0\ 1\ 0, \tag{6}$$

where 1 represents a transmitting slit position and 0 an opaque slit position, to yield a specific set of equations representing the seven detector outputs as

$$D(1) = E(2) + E(3) + E(4) + E(6) + e(1),$$

$$D(2) = E(3) + E(4) + E(5) + E(7) + e(2),$$

$$D(3) = E(1) + E(4) + E(5) + E(6) + e(3),$$

$$D(4) = E(2) + E(5) + E(6) + E(7) + e(4),$$

$$D(5) = E(1) + E(3) + E(6) + E(7) + e(5),$$

$$D(6) = E(1) + E(2) + E(4) + E(7) + e(6),$$

$$D(7) = E(1) + E(2) + E(3) + E(5) + e(7). \tag{7}$$

We can express the detector outputs in matrix form by

$$\mathbf{D}_n = \mathbf{S}\mathbf{E}_n + \mathbf{e}_n, \tag{8}$$

where $\mathbf{S}$ is an S matrix of the order of 7 given by

$$\mathbf{S} = \begin{bmatrix} 1 & 1 & 1 & 0 & 1 & 0 & 0 \\ 1 & 1 & 0 & 1 & 0 & 0 & 1 \\ 1 & 0 & 1 & 0 & 0 & 1 & 1 \\ 0 & 1 & 0 & 0 & 1 & 1 & 1 \\ 1 & 0 & 0 & 1 & 1 & 1 & 0 \\ 0 & 0 & 1 & 1 & 1 & 0 & 1 \\ 0 & 1 & 1 & 1 & 0 & 1 & 0 \end{bmatrix}. \tag{9}$$

We can find an estimate for the energy $\langle \mathbf{E}_n \rangle$ by

$$\mathbf{E}_n = \mathbf{S}^{-1}(\mathbf{D}_n - \mathbf{e}_n), \tag{10}$$

$$\langle \mathbf{E}_n \rangle = \mathbf{S}^{-1}\mathbf{D}_n. \tag{11}$$

In this case estimating the energy of the spectrum requires matrix multiplication by an inverse S matrix. The difference between the estimate and the energy is given by

$$\langle \mathbf{E}_n \rangle - \mathbf{E}_n = \mathbf{S}^{-1} \times \mathbf{e}_n \approx \sqrt{N}e, \tag{12}$$

where N is the number of spectral elements and e is the average noise of a single detector element.[6] We can use Eq. (12) to form an expression for the theoretical S/N expected from the multislit spectrometer as

$$S/N_{multislit} = [(N/2) \times \mathbf{E}_n]/\mathbf{e}_n. \tag{13}$$

The factor of $N/2$ is a result of $N/2$ open slits, which image radiation onto the detector array. We can determine the theoretical S/N improvement obtained with the multislit instrument by taking the ratio of the single slit and multislit S/N's from Eqs. (4)

and (13):

$$\frac{(S/N)_{\text{multi slit}}}{(S/N)_{\text{single slit}}} = \frac{\frac{(N/2)E}{\sqrt{N}e}}{\frac{E}{e}} = \frac{\sqrt{N}}{2}. \qquad (14)$$

The above formulation assumed perfect imaging of the entrance mask onto the focal plane for all wavelengths. However, optical aberrations limit the quality of the image. The degree of aberration varies for different wavelengths, since different wavelengths are imaged onto the detector array from different entrance-mask slit positions. In addition, we have assumed a shift-invariant system. Anamorphic magnification in a real instrument causes deviation from our theoretical construction. When the effects of optical aberration and anamorphic magnification are included in the analysis, the energy distribution at the detector array may be given as

$$\mathbf{D}_n = \mathbf{W}\mathbf{E}_n + \mathbf{e}_n, \qquad (15)$$

where $\mathbf{W}$ is a matrix containing the actual weighting coefficients corresponding to the real instrument.[6]

Instrumentation and Experimental Arrangement

The instrument is shown in Fig. 2. Construction of the instrument was based on an $f/2$, 300-mm radius-of-curvature, holographic grating. The entrance mask comprises 501 adjoining slit positions, each 50 μm wide by 1.5 mm high. The spatial encodement of the entrance mask is based on an $N = 251$ cyclic S matrix constructed by the quadratic residue method.[6] The detector array is an EG&G RL1024SAF silicon photodiode array, consisting of 1024 photodiodes, each 25 μm wide by 2.5 mm high. The system has a spectral range of 737–953 nm with a theoretical resolution of 0.9 nm. The grating was designed on a

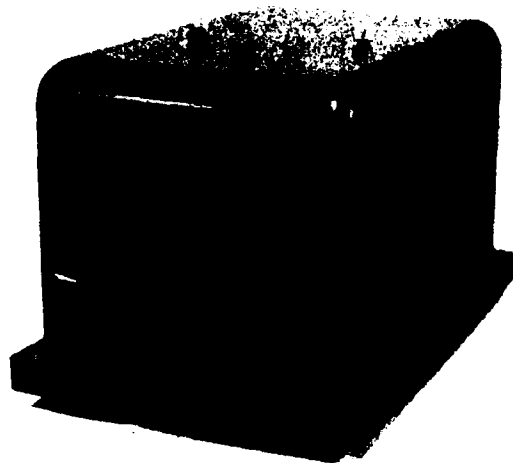Rowland circle.[7] The entrance mask was formed on a flexible film to allow for the required curvature, while a curved focal plane was achieved by a concave spherical fiber-optic faceplate. The integration time of the detector array was set at 180 ms. Array readout was implemented with a Keithley analog-to-digital converter in an IBM AT personal computer.

The experimental arrangement is presented in Fig. 3. A variable power tungsten lamp was filtered by an 806-nm (13-nm full width at half-maximum) interference filter and used to illuminate a diffuse transmitting screen in front of the spectrometer's entrance mask. The size of the illuminated area was controlled to match the acceptance angle of the spectrometer.

Adjacent diodes in the 1024 array were summed to form an equivalent 512-pixel array. A segment that corresponded to a 251-element sample was selected from the 512 data points after calibration with a xenon pen-lamp line source. Further preprocessing consisted of subtraction of the detector dark voltage, which we obtained the dark voltage by blocking the entrance mask and taking a detector-output voltage file. The data were then multiplied by an inverse S matrix to decode the Hadamard-encoded spectral information.

We used a xenon pen lamp for absolute wavelength calibration and also to determine the spectral resolution. The pen lamp was constructed from 6-mm-diameter quartz tubing and is 50 mm in length. This shape permitted us to locate the lamp directly in front of the entrance mask in a horizontal orientation, providing relatively uniform illumination across the entrance mask. We ensured the use of all the instrument's acceptance angle by inserting a diffuser between the lamp and the entrance mask.

Data and Analysis

Xenon Pen-Lamp Source

Spectra obtained from the xenon pen lamp in single-slit and multislit configurations are presented in Figs. 4 and 5. Analysis of the prominent line at 883 nm yields a spectral linewidth of 2.5 nm. The single-slit spectra yield a linewidth of 2.4 nm for the same line;
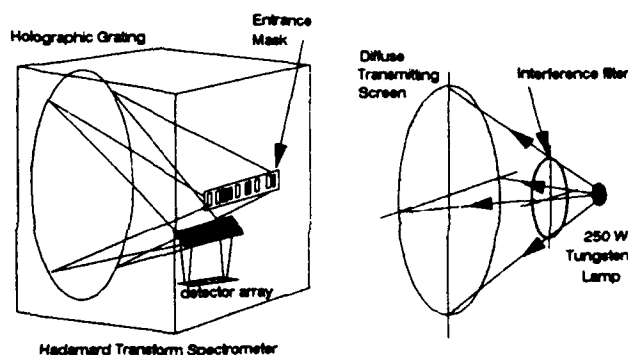

Fig. 2. Hadamard transform spectrometer.

Fig. 3. Experimental layout of the HTS with a narrow-bandpass filtered source.
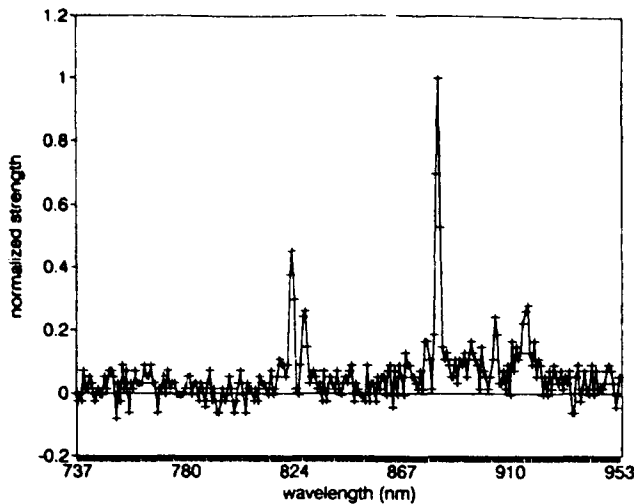
Fig. 4. Xenon pen-lamp spectra obtained with a 100-μm single-slit spectrometer.

Fig. 6. Typical detector output encodegrams for the narrow-bandpass filter source at two different source strengths. The mean value of each encodegram has been removed for display.

however, this spectral width was obtained with a 100-μm slit width, as opposed to the 50-μm slit widths used in the multislit mask. This apparent loss of resolution with the multislit mask may be attributed to the optical aberration of the imaging properties of the concave holographic grating. The instrument requires imaging of a 25-mm object with uniform dispersion, magnification, and blur size. Any deviation from perfect optical performance results in a reconstructed spectra with noise-broadened spectral features.

Narrow-Bandpass Filter Source

The data taken with the narrow-bandpass filtered source yielded detector outputs as displayed in Fig. 6. This detector output, or encodegram, is a result of the superimposition of many images of the Hadamard-encoded entrance mask at the focal plane. A number of reconstructed spectra obtained with different illumination levels are presented in Fig. 7. The spectral features away from the peak centered at 806
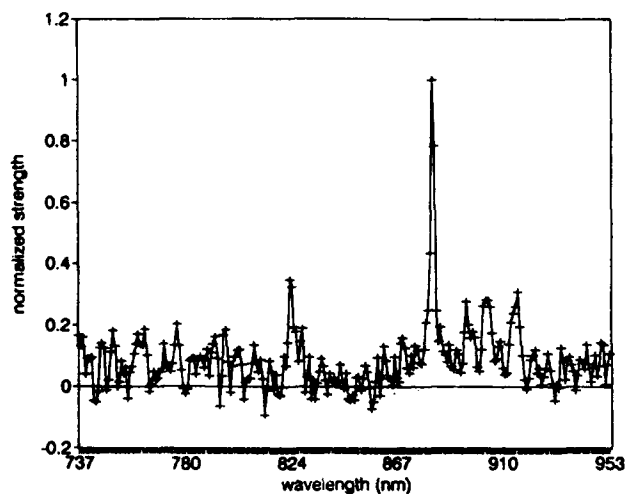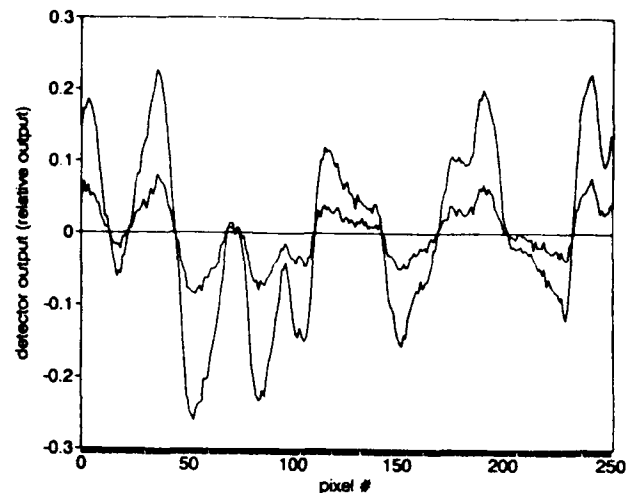
nm are ghosts. The single-slit (100-μm) spectra were obtained directly from the detector output after the multislit entrance mask was replaced with a single-slit entrance mask. The single-slit spectra obtained with the same three illumination levels are presented in Fig. 8.

Noise Sources

A comparison of the single-slit and multislit spectra shows that the spectral noise in the two instruments has quite different characteristics. The single-slit spectra have a noise distribution that appears to be relatively constant as the source strength is increased. However, the noise in the multislit spectra increases with the source strength. This observation is quantified in Fig. 9 where the 100-μm, single-slit and 50-μm, Hadamard-encoded multislit instruments are used to obtain a number of different S/N's versus source strength. The source strength was measured

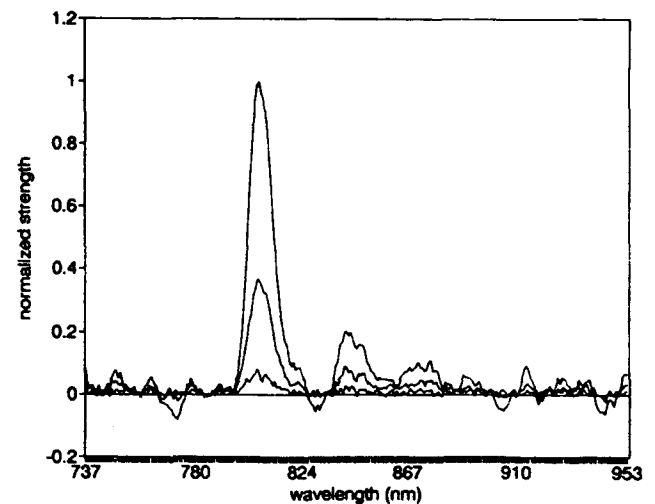Fig. 5. Xenon pen-lamp spectra reconstructed from the HTS.

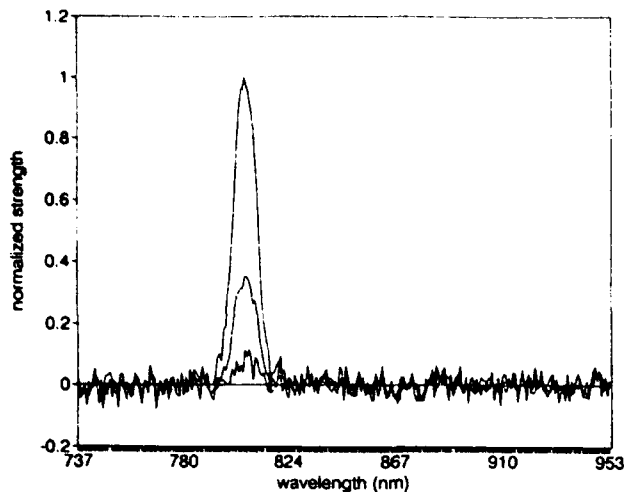Fig. 7. Reconstructed spectra obtained from the HTS with three different source strengths.

Fig. 8. Single-slit spectra obtained with the same three source strengths as in Fig. 7.

with a silicon photodiode on a relocatable stage. The single-slit S/N increases linearly with source strength for the full range of source levels examined. The multislit spectra S/N increases with source strength at a faster rate than the single-slit spectra but then levels off at a S/N of ~18. The single-slit spectra S/N improves linearly, since the main source of noise is detector noise, which is relatively constant. The dark voltage of the detector array was obtained and removed from each detector output file. However, the dark voltage was found to fluctuate with time. It is this dark-voltage fluctuation that represents the main source of noise in the single-slit detector instrument.

Under low illumination levels this dark-voltage fluctuation is the dominant source of noise for the multislit instrument, and accordingly the multislit instrument S/N increases as the source strength

increases and overcomes the dark-voltage variation. In source strength regions above 70 μW m² another noise mechanism begins to dominate and limits the HTS S N. The spectral noise begins to increase proportionally with the peak signal strength. This noise is attributed predominately to optical aberrations.

Systematic errors in the instrument can be thought of as encodegram error. A number of mechanisms exist that cause the encodegrams to deviate from the idealized imaging assumed in our theoretical analysis. The layout of the instrument demands off-axis imaging of the entrance mask. This imaging results in nonuniform blurring for different portions of the mask, which varies with wavelength, since different portions of the entrance mask are used for different wavelengths. Anamorphic magnification and stray light are other noise sources that are correlated with the encodegram and therefore with the wavelength of the test source. Additionally, some portion of the noise consists of anomalous spectral lines or ghosts.[8] The strength of these encodegram errors increases as the source strength increases. They eventually limit the HTS application in strong-illumination-level situations.

We determined the effect of the detector dark-noise fluctuation on the spectra by sampling 100 dark-voltage outputs. One output file has been subtracted from the others to yield 99 files that contain information about the detector-array, dark-voltage variation with time. The average value of the standard deviation of each detector over the 99 samples was taken and used along with the peak value of the multislit spectra to construct a S/N. This S/N is plotted in Fig. 9(c) and emulates the multislit instrument's performance based on detector noise only. Note that the S/N curve constructed has a slope that is similar to the multislit S/N in the low-source-strength regions.

In Fig. 10 we compare S/N's for the same slit widths in single-slit and multislit configurations.
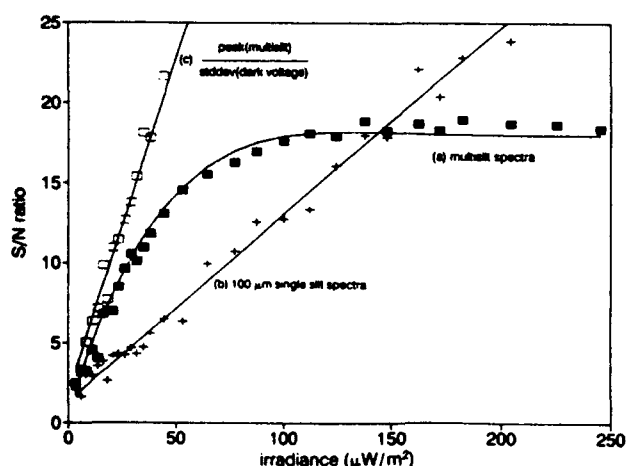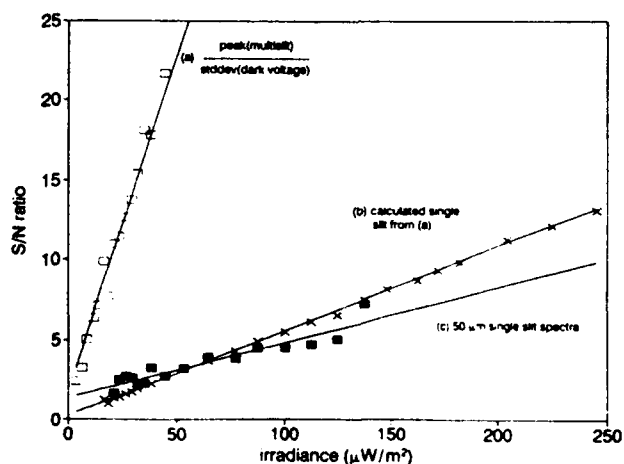

Fig. 9. Comparison of the S/N's obtained in (a) multislit and (b) single-slit configurations as a function of source irradiance. A third S/N is constructed from the multislit peak signal and a detector dark-voltage term (c) as described in the text. This third S/N (c) simulates the performance of a HTS, which is S/N limited by detector dark-voltage temporal variation.

Fig. 10. Comparison of the single-slit S N obtained with a 50-μm entrance slit (c) and the same S N as calculated (b) from the detector dark-voltage-limited multislit S N (a).
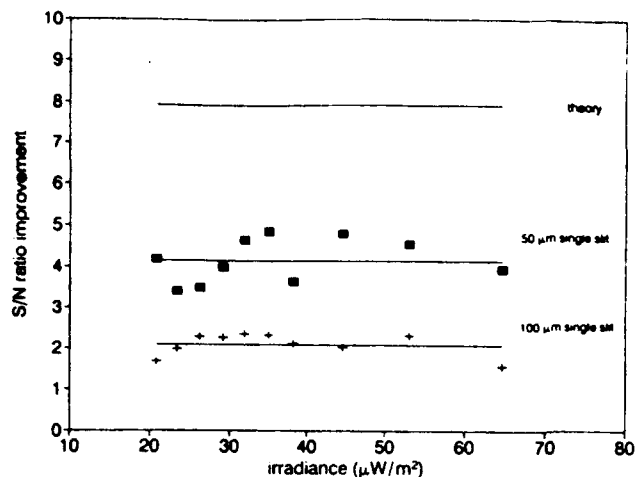
Fig. 11. S/N improvement obtained with the HTS compared with the 50-μm, single-slit spectrometer, the 100-μm, single-slit spectrometer, which has comparable resolution, and the theoretical limit of $n^{1/2}/2$.

Curve (a) is transferred from Fig. 9 and is the multislit instrument's S/N based on detector noise only. Curve (b) represents the calculated single-slit performance when curve (a) is divided by $N^{1/2}/2$. Curve (c) shows the actual test data for a 50-μm single-slit configuration. There is fairly good agreement between the calculated and measured S/N's for the single-slit configuration.

The S/N improvement can be better quantified by Fig. 11. Here we ratio the multislit S/N to the single-slit S/N for the low illumination levels where the multislit instrument seems to yield an improvement ($L_{source} \leq 70 \ \mu W/m^2$). The comparison with the 50-μm single slit yields an improvement of ~4.14, while the comparison with the 100-μm single slit yields an improvement of 2.08, as opposed to the theoretical factor of 7.92.

Conclusion and Comments

The constructed HTS displays the capability of simultaneously capturing spatially encoded spectral information. The encoded spectrum of a xenon line source and a broader 13-nm interference filter source have been successfully reconstructed. In conditions of low illumination levels the multislit instrument displays a S/N improvement of a factor of 2.08 over a single-slit instrument with the same spectral resolution.

Our analysis of the data suggests that we may improve the performance of the breadboard multislit instrument by enhancing the performance of the optical system. A more advanced optical design that would better image the extended entrance mask onto the focal plane would improve the multislit instrument's spectral resolution and limit encodegram error, increasing the system's upper S/N limit. Harwit and Sloane[6] have discussed the need for excellent imaging over the wide field of the entrance aperture with a minimum of aberrations. The current optical design does not meet these important requirements

and would be better replaced by a wide-field corrected Czerny–Turner configuration.[6] The multislit instrument was also examined with an N = 503, 50-μm slit-width entrance mask. The performance of the HTS in this configuration was very limited since the effects of optical aberration, anamorphic magnification, and second-order diffraction combined to degrade the performance of the multislit instrument severely.

Note that we attempted an alternative technique to decode the spectral information from the spatially encoded data. The spectral data presented here were decoded by transformation of the spatially encoded voltage outputs by a binary S matrix. The S matrix consisted of ones and zeros exclusively, assuming perfect optical imaging, linear shift invariance, and uniform detector and grating efficiencies. We attempted to replace the binary S matrix with a weighted W matrix that contains the actual weighting coefficients corresponding to our instrument's imaging and dispersion properties. We constructed the W matrix by obtaining an encodegram at each of the instrument's 251 spectral elements. These 251 data files were obtained with a monochromator with a xenon arc lamp as a calibrated source in an f/2 configuration. Application of this inverse W matrix has resulted in successful reconstruction of any of the 251 data files obtained in this original data set; however, application of the W matrix to any unknown, polychromatic source results in a spectrum that contains no recognizable spectral information.

The poor performance of the W-matrix transformation is attributed to the fact that the HTS does not possess the circulant properties that were demanded in the theoretical model. The theoretical application of the S matrix to decode the spectra demanded a circulant matrix where each row could be obtained by any other row after a linear shifting of the elements. The W matrix obtained comprises individual encodegrams that vary in amplitude by as much as a factor of 3 because of the differences in grating efficiency and detector responsivity. In addition, the spatial variation of each encodegram is different because of the nonuniform dispersion and blurring of each of the different slit positions. Furthermore, our film mask is neither perfectly opaque nor perfectly transmitting, and random noise is also present from detector dark-current variation and optical cross talk. Simulation of an N = 7, Hadamard-encoded system has shown that as the W matrix departs from the circulant properties present in the S matrix the quality of the spectral reconstruction degrades. We believe that the variation of the different encodegrams used to make up this instrument's W matrix is significant enough to make reconstruction of the spectral information impossible. Application of the W-matrix technique requires an instrument with similar spectral responsivities and a more uniform point-spread function across the entrance mask.

References

1. J. A. Decker, Jr., "Experimental realization of the multiplex advantage with a Hadamard transform spectrometer," Appl. Opt. 10, 510–514 (1971).

2. M. J. E. Golay, "Multi-slit spectrometry," J. Opt. Soc. Am. 39, 437–444 (1949); "Static multislit spectrometry and its application to the panoramic display of infrared spectra," J. Opt. Soc. Am. 41, 468–472 (1951).

3. N. J. A. Sloane, "Reducing the number of measurements in doubly multiplexed spectrometers," in *Proceedings of the Aspen International Conference on Fourier Spectroscopy, 1970*, G. A. Vanasse, A. T. Stair, and D. J. Baker, eds. (Air Force Cambridge Research Laboratories, Hanscom Air Force Base, Mass., 1971), pp. 435–440.

4. R. A. Van Tassel and W. K. Wong, "Hadamard-coded, stationary-entrance-mask, photodiode-array spectrometer," in *International Conference on Fourier Transform Spectroscopy*, D. G. Cameron, ed., Proc. Soc. Photo-Opt. Instrum. Eng. 1145, 384–390 (1989).

5. J. L. Robichaud, W. K. Wong, and R. A. Van Tassel, "Measured performance of a Hadamard-coded photodiode-array spectrometer," in *Eighth International Conference on Fourier Transform Spectroscopy*, H. M. Heise, E. H. Korte, and H. W. Siesler, eds., Proc. Soc. Photo-Opt. Instrum. Eng. 1575, 255–257 (1992).

6. M. Harwit and N. J. A. Sloane, *Hadamard Transform Optics* (Academic, New York, 1979).

7. H. A. Rowland, "On concave gratings for optical purposes," Am. J. Sci. 26(3), 87–98 (1883).

8. M. H. Tai, M. Harwit, and J. A. Sloane, "Errors in Hadamard spectroscopy or imaging caused by imperfect masks," Appl. Opt. 14, 2678–2686 (1975).